RUJCST
ISSN-L 3007-5084
جامعة الرازي
Al-Razi University
كلية الحاسوب وتقنية المعلومات
مجلة جامعة الرازي لعلوم الحاسوب وتقنية المعلومات
Al-Razi University Journal of Computer Science and Technology
علمية محكمة تصدر عن كلية الحاسوب وتقنية المعلومات - جامعة الرازي

Early Diagnosis of Multiclass Skin Lesions Using Hybrid Models Based on Fused Features

Ebrahim Mohammed Senan

Department of Information Syetem, Faculty of Computer Science and Information Technology, Alrazi University,Sana'a, Yemen
senan1710@gmail.com

Khalil Al-Wagih

Department of Artificial Intelligence, Faculty of Computer Science and Information Technology, Alrazi University,Sana'a, Yemen
khalilwagih@gmail.com

Eman A. Alshari

Department of Information Syetem, Faculty of Computer Science and Information Technology, Alrazi University,Sana'a, Yemen
em.alshari3@gmail.com

Abstract—**Skin lesions (SL) are among the most serious types of skin diseases. Melanoma is considered a serious type of skin lesion. The incidence of melanoma increases annually, which poses a health risk. Life threatening. Dermoscopy is one of the best techniques that reveals invisible internal structures and helps detect types of SL. The SL are similar in the early stages, which poses a challenge to distinguish between them by manual diagnosis. Therefore, artificial intelligence (AI) techniques address deficiencies through manual diagnosis. In this study, two strategies were developed to analyze dermoscopic images for early diagnosis of SL. The images were optimized for ISIC 2018 and the Active Contour Algorithm (ACA) was applied to extract regions of interest (ROI) and isolate them from healthy areas. The ROI was fed to two strategies separately. The first strategy received the ROI and was fed to the Gray-Level Co-occurrence Matrix (GLCM), Local Binary Patterns (LBP) and Fuzzy Color Histogram (FCH) algorithms to extract features. They were combined into feature vectors. The fused features were fed to the Artificial Neural Network (ANN) and Support Vector Machine (SVM) classifiers to classify them with high accuracy. The second strategy received the ROI and fed it to the ResNet18 model to extract the deep features and classify them with great efficiency using ANN and SVM. ANN-ResNet18 achieved promising results, reaching an AUC of 84.73%, sensitivity of 87.74%, accuracy of 93.8%, precision of 82.9%, and specificity of 98.47%.**

Keywords—***CNN; ANN; SVM; Fusion features; Skin Lesion; HF***

I. INTRODUCTION (*HEADING 1*)

The skin is the largest organ in the human body and serves as a line of defense against external dangers such as physical infections, ultraviolet rays, and pathogens [1]. Skin diseases are considered a public health problem because it increases the mortality rate if it is not diagnosed in their early stages [2]. The skin regulates temperature at a constant level, gives the body immunity against pathogens, and prevents dehydration. Skin pigmentation varies from person to person depending on weather conditions, from cold to hot. Skin type ranges from dry to oily [3]. Due to DNA damage, it leads to abnormal cell growth and causes skin cancer (SC). Exposure to ultraviolet rays for a long period of time is one of the most important causes of SC. Family history and age are also causes of SC [4]. People with light skin are more susceptible to SC due to a decrease in melanin, which is responsible for protecting the skin from ultraviolet rays. Surgical operations to remove infected tissue are considered effective, especially in the initial stage. Radiotherapy and chemotherapy are also ways to treat SC [5]. The Dermoscopy magnifies skin diseases, including pigment networks and all the features in the diseases. Enhancing structures provides an opportunity for experts to distinguish all types of diseases (melanocytic and non-melanocytic) and detect malignant lesions. Diseases are diagnosed in two separate parts: global and local features and each part has features [6]. Global features allow experts to have a rapid ability to diagnose a disease. The global features are the grid pattern, defined by a brown network with a gray-brown background, a spherical pattern with shapes of different sizes, round, oval colors, and a pattern with star lines at the edges [7]. Local features are used to diagnose diseases and identify the type of disease, using medical algorithms to diagnose skin diseases. Local [8]. To identify skin diseases in dermoscopy images, dermatologists analyze and compare lesion features and characteristics to detect the type of lesion and give appropriate treatment. The similarity of features early in the lesion presents a challenge for manual diagnosis by expert dermatologists. Several diagnostic techniques have been used for SL, such as ABCD, 7-point checklist, pattern analysis, and Menzies method. Machine and deep learning (DL) techniques help address the challenge of manual diagnosis limitations, especially in the early stages [9]. Machine learning (ML) and DL systems have achieved superior results for diagnosing SL, helping doctors save patients' lives. Convolutional Neural Network (CNN) models work with high accuracy by analyzing theaterscopic images to extract hierarchical features such as edges, color, shape, and

complex patterns [10]. It also has the superior ability to analyze thousands of images with high accuracy and speed. Hybrid techniques combine the strengths of ML and DL to efficiently and accurately diagnose SL [11]. In this study, features are extracted using hybrid algorithms and classified using CNN and ML classifiers. Hybrid techniques between ML and DL are also applied, where features are extracted by DL and classified by ML.

The most important contributions as follows:

- Isolation of the areas of pests and distortions from healthy skin.
- Handcraft extract by combining three GLCM, LBP, and FCH algorithms.
- Application of hybrid technology between ANN-ResNet18 and SVM- ResNet18 to diagnose images of lesions skin.

The rest of the paper as follows: Section 2 analyzes the methods of previous studies. Section 3 explains the methods and tools used in this study to diagnose SL. Section 4 presents the results of the proposed strategies to diagnose SL. Section 5 discusses and compares the performance of the proposed systems with previous studies. Section 6 concludes the study.

II. Related work

This section reviews the methodologies and performance of previous studies.

Soudani et al. presented VGG-16 and ResNet-50 models for skin lesion classification. The images are enhanced through the downsampling method. The dropout method was used to avoid overfitting. VGG-16 and ResNet-50 got an accuracy of 76.3% and 73.2% [12]. Liu et al. presented a system to segment the lesion region. The system consists of encoder blocks and a decoder. Applying the Retinex method to enhance color consistency between different dermatoscopy images. Feature extraction was done using ResNet and DenseNet and dimensionality reduction was done using PCA [13]. Pollastri et al. presented a method to segment lesions and separate them from the healthy body. Data augmentation for the lesion area segmentation task has been done using Generative Adversarial Networks. The Deep Convolutional-GAN (DCGAN) method was used. DCGAN has four convolutional layers and a kernel size of 5x5 [14]. Mabrouk et al. presented a system for detecting SL, resizing and adjusting images, adjusting contrast, enhancing images, and removing all unnecessary pixels. Density regression was applied to determine the intensity of the pigmented network and identify the lesion according to the specified threshold value. The features extracted from the lesion area were fed to SVM, KNN and ANN classifiers. The system achieved the highest accuracy using ANN with texture features with an accuracy of over 90% with clinical images [15]. Gong et al. introduced transfer learning to fine-tune a CNN to extract skin lesion features. The images were normalized to control differences in lighting, color, angles, etc. The classification was done by ensemble learning CNN. The network achieved an accuracy of 90.4%, sensitivity of 45%, and specificity of 93.7% [16]. Birkenfeld et al. presented the Otsu method for skin lesion segmentation. Features were extracted from lesion region using the ABCD rule. The features extracted by the ABCD rule were fed into the logistic regression classifier. The logistic regression method was used to balance the data. The system reached a sensitivity of 83.2% [17]. Fekry et al. presented a system for diagnosing SL. The images were enhanced, segmented, and features extracted using CNN. Classification was done using an RF network, which achieved an AUC of 87.98%, and sensitivity of 80.4%, [18]. Naeem et al. presented a methodology for classifying dermatoscopy images. Anisotropic diffusion was applied to enhance the images and normalize the dataset by SMOTE. Features were extracted and classified using the VGG19 model. VGG19 got an accuracy of 77.97% and a sensitivity of 69.49% [19]. Ahmad et al. proposed a DL that combines VGG16 and CNN for skin lesion classification. AlexNet got an accuracy of 93.14% [20]. Kaur et al. proposed a CNN using sharp convolutions for automatic lesion segmentation. The network was designed from scratch using convolutional layers with different filters, water leakage activation, batch normalization, and parameter tuning. With ISIC2016 images, the network achieved an average Jaccard of 90.4%, and with ISIC2018 images, it achieved an average Jaccard of 89.1% [21].

The researchers dedicated their efforts to achieving superior results for image diagnosis on the ISIC2018 dataset. Ultra-resolution remains the goal of all researcher. It is noted from previous studies that there is a scientific gap related to the lack of hybrid algorithms for feature extraction. Therefore, this study will address the gap by extracting features in several ways and combining them into common vectors.

III. Methodology

The section describes the methodology for analyzing images of the ISIC 2018 dataset for diagnosing SL, as in Figure 1. The images were first enhanced and lesion areas isolated from healthy areas using the ACA algorithm. The features were extracted using two methods: first, using the traditional algorithms GLCM, LBP and FCH and merging them together. The fused images were diagnosed by ANN and SVM. Secondly, extracting deep features using ResNet18 and diagnosing them using ANN and SVM classifiers.

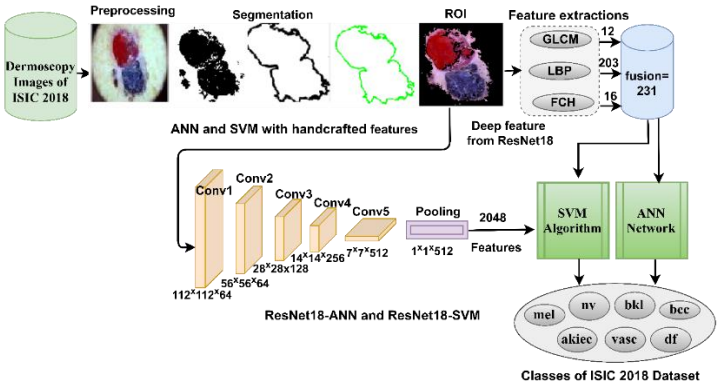

Fig.1. Hybrid methodology for image analysis of the ISIC 2018 dataset for skin lesion diagnosis.

A. Description of ISIC 2018 Dataset

The ISIC 2018 dataset is part of the ISIC initiative, aiming to diagnose SL using imaging and artificial intelligence techniques. The dataset is publicly available and available for researchers to evaluate the performance of their systems [22]. The dataset includes more than 10,015 dermatoscopy images showing various SL in different locations. The ISIC 2018 dataset includes seven types of SL. melanocytic nevus (NV) 6705 images, melanoma (MEL) 1113 images, basal cell

carcinoma (BCC) 514 images and actinic keratosis (AKIEC) 327 images and benign keratosis (/ seborrheic keratosis / lichen planus such as keratosis) (BKL) 1099 images, dermatofibroma (DF) 115 images, and vascular lesion (VASC) 142 images.

B. Enhancement of Dermoscopy Images

Preprocessing images is the first step to image improvement. The acquired images contain noise, artifacts, and low contrast. So the main motive of pre-processing is to remove artifacts, improve low contrast, and remove air bubbles and skin lines. The presence of some image artifacts leads to blocking an vital part of the skin lesion and creating false features. In this study, a Gaussian filter was used to improve the images and ensure the efficiency of the systems in the next stage and accurate diagnosis. Dermoscope images contain artifacts caused by factors such as hair, skin lines and air bubbles [23]. All this noise is present in images, which affects the accuracy of the system's diagnosis. Gaussian filter is one of the filters that improves image quality and removes unwanted pixels. Gaussian filter removes all unwanted pixels, and calculates the average value of neighboring pixels using a 2D convolution operator [24]. Noise is removed, and images are improved. In Equation 1, it is known as the Gaussian equation to improve images by removing unwanted noise and impurities. Figure 2.b shows a group of dermatoscopy images of different types of SL.

$$h(x,y) = \frac{1}{2\pi\,\sigma^2}\, e\, \frac{x^2-y^2}{2\sigma^2} \qquad (1)$$

where x and y are the coordinates in two-dimensional space and σ is the standard deviation of the Gaussian distribution.

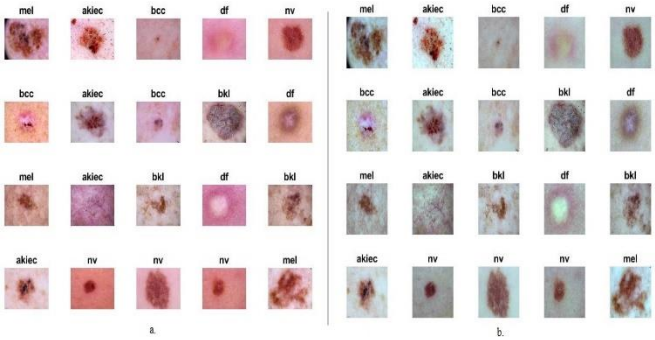

Fig. 2. Samples from the ISIC 2018 dataset a. Before enhancement b. After enhancement.

C. Active Contour Algorithm

The segmentation phase is important and difficult phases in image processing. It must be accurate because the following steps depend on analyzing the segmented region only. The image contains lesion region and healthy areas, so segmentation separates the lesion areas, called regions of interest (ROI), from the healthy areas. Low contrast, reflections, air bubbles, and skin and hair lines make segmentation a difficult task. In this study, the ACA was applied to separate lesional region from healthy skin. ACA works by segmenting lesion region from input images. Active contour is defined as a pattern that separates the ROI pixel area from the background to obtain highly efficient diagnostic results [25]. ACA has the superior ability to extract pest boundaries. Contour is the boundary for the purpose of defining the lesion area. It is a set of points whose work is subject to an interpolation process. It is linear or polynomial and can define the boundaries of the lesion. ACA is a process that describes lesion edges and other features to form contour and curve patterns. The curve patterns are determined through using internal and external forces through Equation 2 [26]. These forces are related to the image curves. External energy is the combination of energy that controls positioning within the image. The deformational changes are controlled by internal energy.

$$G_{cv}C = \int_{outside} (I(x) - m_1)^2\, dx + \int_{inside} (I(x) - m_2)^2\, dx + \beta length\,(C) \qquad (2)$$

Where I mean gray intensity, *m1 is* power outside, *m2* is power inside, β is a parameter, *length(C)* Indicate the length of contour C and *G* makes the contour evolve to the boundary of the object. Figure 3 describe some images of different types of SL. after segmentation.

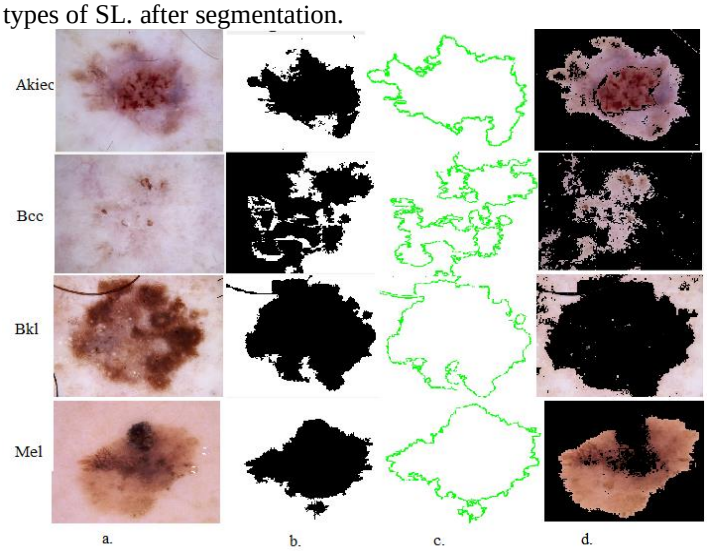

Fig.3. describe some images of different types of SL a. Original images b-c. After segmentation d. ROI.

D. Morphological Method

The morphological method is an image processing method to enhance images and improve the performance of subsequent image processing operations. When applying segmentation algorithms, segmentation leaves very small holes in the ROI and these holes do not belong to the skin lesion, so these holes should be removed to obtain an enhanced image. The input images to the morphological method are binary images, and the output is an enhanced binary image [27]. The presence of these holes negatively affects feature extraction, so morphological methods were applied to remove these distortions from dermoscopic images while preserving the shape and size of the images. The morphological method is a set of linear processes based on shape. It depends on the distribution of the relative pixel values, so it is suitable for binary images. The method works to explore a small template called the structure element. The method places the structure element on each image location and compares it with neighboring pixels. The process tests whether the structure element fits within the neighborhood or not, while the other tests the intersection in the neighborhood and is called hits [27]. The morphological method works on binary images and

produces an enhanced binary image. Figure 4 describe some images of different types of SL after morphological methods.

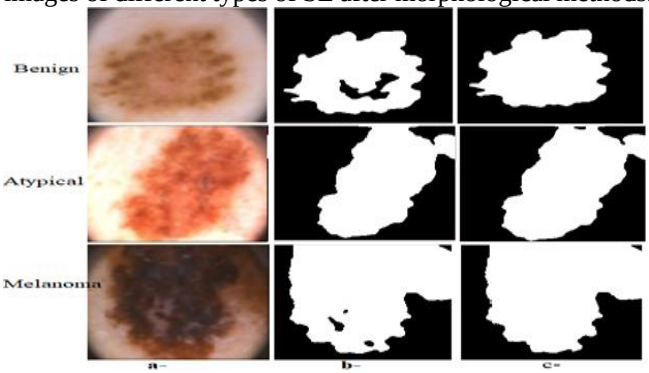

Fig.4. Results of the proposed system performance a. Original images b. Segmentation c. Morphological

E. Features Extraction Methods

An image contains many different colors, textures and shapes and has thousands of features, so it is important to extract the important features from the image, to reduce the image dimensions and speed up the calculation process. In diagnostic systems, features are extracted from the ROI, which is identified through a segmentation process. Diagnostic systems rely mainly on extracting the important landmarks from the lesion area. Classifiers will not be able to diagnose correctly if features are extracted poorly [25]. The primary goal of feature extraction is to improve the effectiveness and efficiency of accurate detection and diagnosis. Feature extraction is the basic step in building classifiers for pest diagnosis, and feature extraction operations aim to extract features related to each class and store them in feature vectors. There are many features in the area of SL, the important of which are color, shape, and texture. There are many algorithms used for feature extraction. In this study, features were extracted using the GLCM, LBP, and FCH algorithms, and then all features were combined to form highly representative features for each image [28].

The GLCM algorithm examines texture by examining the spatial relationships of pixels. It measures the number of times that pairs of pixels that have specific values and spatial relationships appear. A GLCM matrix is constructed such that each element of the matrix (i, j) represents the frequency of the value of pixel i at a certain distance d and direction θ from pixel j. Texture features that represent 12 features such as contrast, correlation, homogeneity, energy, and others are calculated.

The LBP algorithm operates on a 2D texture descriptor that measures local contrast and local texture pattern. The features of the skin lesion are extracted by analyzing the central pixel and replacing it with mathematical pixels according to Equation 3 [29]. The central pixel g_c and the adjacent pixel g_p are compared. The LBP algorithm extracts 203 from each ROI of the skin lesion.

$$LBP\,(x_c, y_c)_{R,P} = \sum_{P=0}^{P-1} s\big((g_p - g_c).2^P \qquad s(x)$$
$$= \begin{cases} 0, & x < 0 \\ 1, & x \geq 0 \end{cases} \qquad (3)$$

where *R* means the radius for neighbouring, R and *P* points on the circle of radius R, 2^P a weight is given to each P-th comparison in the binary pattern, P represent the number of neighbours and s(x) is a threshold function.

The FCH algorithm works by fuzzy logic so that the colors in the image are distributed into histogram bin areas. FCH analyzes the color similarity of an image through the total membership value of each pixel and the distribution of pixels over the total histogram bins.16 features were extracted from each skin lesion ROI.

F. Fusion of Features

Features fusion is a process that combines multiple features into one vector feature for accurate diagnostic accuracy. The main goal of the method is to obtain high performance in diagnostic systems. In diagnosing medical images, there are problems and obstacles in diagnostic accuracy, which can be solved by the fusion method by combining a set of features extracted by several methods and combining them into one feature vector. In the proposed system, the features were extracted by three algorithms, then combined and stored in one feature vector for each image and one feature matrix for all images called a new dataset. These feature matrices are a hybrid of G LCM, LBP, and FCH features. After integrating the features of the three algorithms, a feature matrix with a size of 231 features is produced which called handcrafted features (HF), as shown in Figure 5.

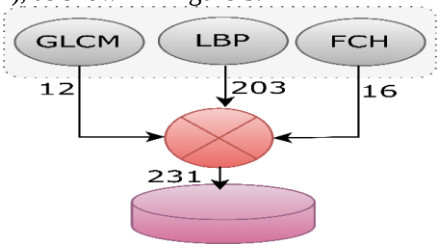

Fig.5. Fusion of HF

G. CNN for Extraction of Deep Features

CNNs consist of a set of blocks, each block containing a set of layers (convolutional, pooling, fully connected). The main objective of the convolutional layers is to extract the features from the input images that have a 2 D structure. The convolutional layers detect local features in the input feature. When the number of convolutional layers is more, more complex features are extracted [30]. Pooling layers reduce the size of feature maps through average-pooling and max-pooling techniques. Hence, the pooling layers aim to reduce the size of feature maps and parameters and reduce complexity in the network [31]. The fully connected layer is the classification stage in the CNNs to classify the complex features maps extracted from the previous layers. This layer contains many neurons connected with all in sequential layers. Figure 6 shows the classification and deep feature extraction layers [32]. To classify a images of ISIC2018 dataset, the dataset was trained on the ResNet-18 model.

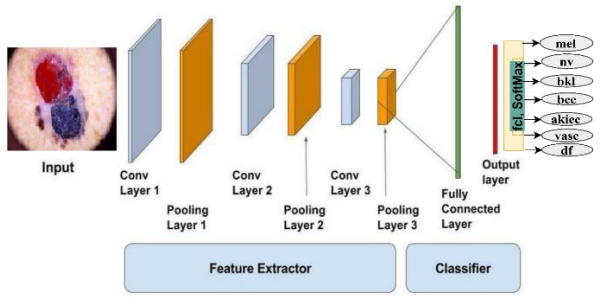

Fig.6. Deep Feature Extraction and Classification Layers.

H. Classification

Classification is the last phase of image processing, as it depends on the accuracy of the previous phases. After extracting features from ROI, each feature in the image is put into a vector, and all images are represented in a feature matrix, which is the input to the classifiers. In this study, an ANN and an SVM classifier were used to classify the ISIC2018 dataset. Classification techniques involve two steps: an inductive step to build a data classification model called data training. Step Two: A deductive step to test the data.

H.1. ANN Network

ANN is a set of layers connected through neurons connected and interconnected by weights. She has a high ability to analyze and interpret complex data and produce clear information and patterns. It has the ability to adapt to changing conditions and environments. ANN minimizes the error to calculate the probabilities of belonging to any other category. Neural networks consist of simple processing units that communicate with each other and send signals to each other through weighted connections. Information in ANN flows from the inner layer to the output layer via hidden layers; Information is propagated between layers and neurons and stored as connected points called weights. The input layer receives data through input units equal to the number of features [33]. Hidden layers analyze and process data and produce patterns through neurons connected and interconnected between the layers. The hidden layers set to 15 hidden layers. Finally, the output layer produces the information, which contains 7 neurons, the number of classes in the data set. Figure 7 shows the ANN infrastructure that receives 231 features fused to the inner layer, analyzes them through 15 hidden layers, and classifies each image through the output of 7 neurons in the output layer [34].

The other strategy is a hybrid between the ResNet18 model and ANN. The ANN algorithm also receives the features extracted from ResNet18 then classifies them.

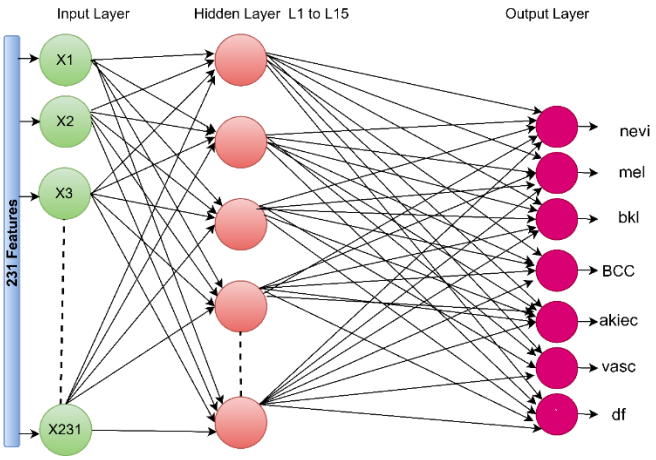

Fig.7. ANN infrastructure for image classification for ISIC 2018 dataset.

H.2. SVM Algorithm

The goal of SVM is to create multiple decision boundaries to separate the data of each class [35]. Hyperplanes are decision boundaries that have the maximum margin. Support vectors are those points that are closest to the hyperplanes. In this study, the SVM receives 231 features for each image and classifies each image according to seven classes, meaning that the SVM works according to one versus all. So that the features are analyzed one against all, and the features of one class are separated from the rest, and the mechanism is repeated until all the features are classified into their classes, {xi i=1,2,……N}, N is a number of classes. Let {xi, yi}, where xi represents data points and yi ∈ {1, -1}, it's corresponding labels [36].

The other strategy is a hybrid between the ResNet18 model and SVM. The SVM algorithm also receives the features extracted from ResNet18 and classifies them.

IV. Results of Systems Performance

A. Splitting ISIC2018 Dataset

Table 1 describes the distribution of the ISIC2018 skin lesion dataset for evaluating the proposed systems into: training, validation, and testing. The data set was divided into 80% for training the proposed models, which was divided into 80% for training and 20% for validation. 20% of the data set was isolated to test the performance of the proposed systems.

TABLE 1. SPLITTING THE ISIC2018 DATA SET OF SL

Phase	**80% (80:20)**		**Testing 20%**
Classes	**Training (80%)**	**validation (20%)**	
Nv	4291	1073	1341
Mel	712	178	223
Bkl	703	176	220
Bcc	329	82	103
Akiec	210	52	65
Vasc	91	23	28
Df	74	18	23

B. Evaluation Metrics

Evaluation metrics are applied to evaluate the proposed systems. There are several metrics to evaluate models, such

as the confusion matrix (CM). The CM consists of equal columns and rows. The number of classes determines the size of the CM. The CM explains the correct and incorrect prediction results of the classification; It is divided into rows of positive and negative actual values and columns of positive and negative forecast values. The performance of the proposed systems was tested as shown in Equations 4-8 [37].

$$\text{AUC} = \frac{\text{TP Rate}}{\text{FP Rate}} \quad (4)$$

$$\text{Accuracy} = \frac{\text{TN} + \text{TP}}{\text{TN} + \text{TP} + \text{FN} + \text{FP}} \quad (5)$$

$$\text{Sensitivity} = \frac{\text{TP}}{\text{TP} + \text{FN}} \quad (6)$$

$$\text{Precision} = \frac{\text{TP}}{\text{TP} + \text{FP}} \quad (7)$$

$$\text{Specificity} = \frac{\text{TN}}{\text{TN} + \text{FP}} \quad (8)$$

C. Results of ANN with HF

The section discusses the performance of ANN with HF for classification on the ISIC2018 dataset. The images were improved, ROI and deformities were isolated, and fed into traditional feature extraction algorithms. The features of the three algorithms are combined into fused feature vectors to form the HF. The HF are fed to an ANN for classification.
Table 2 describes the performance of ANN with HF for classifying the ISIC2018 dataset. ANN achieved an AUC of 84.41%, accuracy of 91.4%, sensitivity of 89.39%, precision of 84.44%, and specificity of 98.34%.

TABLE 2. RESULTS OF ANN WITH HAND-CRAFTED FEATURES FOR CLASSIFICATION ON THE ISIC2018 DATASET

Type of Class	AUC %	Accuracy %	Sensitivity %	Precision %	Specificity %
akiec	89.4	93.8	94.2	87.1	99.5
bcc	88.7	92.2	92.3	92.2	99.5
bkl	87.9	93.2	92.8	96.2	99.8
df	85.2	91.3	91.4	95.5	99.7
mel	87.9	93.3	92.9	64.2	92.6
nv	84.2	91.3	90.7	98.8	98.2
vasc	67.6	71.4	71.4	57.1	99.1
average ratio	**84.41**	**91.40**	**89.39**	**84.44**	**98.34**

Figure 8 shows the CM generated by the ANN with HF to classify the ISIC2018 dataset. The ANN achieved accuracy for each class: akiec of 93.8%, bcc of 92.2%, bkl of 93.2%, df of 91.3%, mel of 93.3%, nv of 91.3% and vasc of 71.4%.

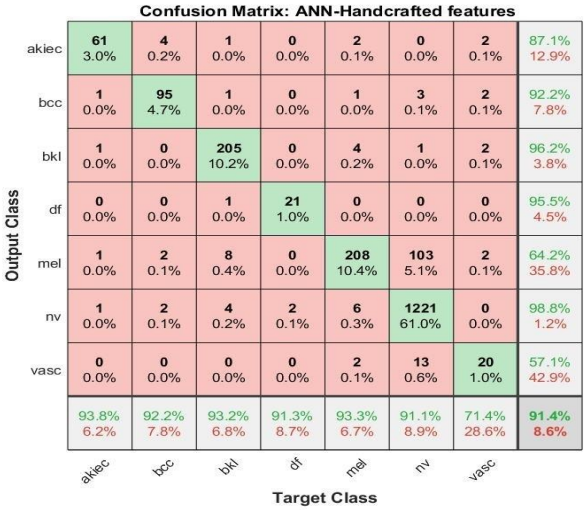

Fig.8. Display CM for results of ANN with HF for classification on the ISIC2018 dataset.

D. Results of SVM with HF

The section discusses the performance of SVM with HF for classification on the ISIC2018 dataset. The images were improved, ROI and deformities were isolated, and fed into traditional feature extraction algorithms. The features of the three algorithms are combined into fused feature vectors to form the HF. The HF are fed to an SVM for classification.
Table 3 describes the performance of SVM with HF for classifying the ISIC2018 dataset. SVM achieved an AUC of 67.94%, accuracy of 83.7%, sensitivity of 71.53%, precision of 74.63%, and specificity of 95.96%.

TABLE 3. RESULTS OF SVM WITH HF FOR CLASSIFICATION ON THE ISIC2018 DATASET

Type of Class	AUC %	Accuracy %	Sensitivity %	Precision %	Specificity %
akiec	62.8	67.7	68.2	61.1	98.5
bcc	58.2	61.2	61.4	77.8	98.7
bkl	80.9	85	84.8	59.2	93.4
df	56.7	60.9	61.5	73.7	99.5
mel	41.2	43	42.9	72.2	98.3
nv	90.3	93	93.2	92.2	83.7
vasc	85.5	89.3	88.7	86.2	99.6
average ratio	**67.94**	**83.70**	**71.53**	**74.63**	**95.96**

Figure 9 shows the CM generated by the SVM with HF to classify the ISIC2018 dataset. The SVM achieved accuracy for each class: akiec of 67.7%, bcc of 61.2%, bkl of 85%, df of 60.9%, mel of 43%, nv of 93% and vasc of 89.3%.

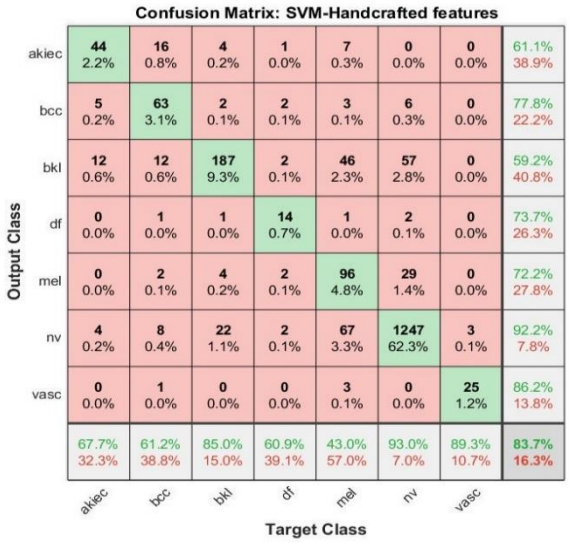

Fig.9. Display CM for results of SVM with HF for classification on the ISIC2018 dataset.

E. Results of ANN with ResNet18 Features

The section discusses the performance of ANN with ResNet18 features for classification on the ISIC2018 dataset. The images were enhanced, ROI and deformities were isolated, and fed into ResNet18 model. The deep features of ResNet18 are fed to an ANN for classification.

Table 4 describes the performance of ANN with ResNet18 features for classifying the ISIC2018 dataset. ANN achieved an AUC of 84.73%, sensitivity of 87.74%, accuracy of 93.8%, precision of 82.9%, and specificity of 98.47%.

TABLE 4. RESULTS OF ANN WITH RESNET18 FEATURES FOR CLASSIFICATION ON THE ISIC2018 DATASET

Type of Class	AUC %	Accuracy %	Sensitivity %	Precision %	Specificity %
akiec	86.7	90.8	90.8	89.4	99.5
bcc	88.6	91.3	91.3	87.9	98.7
bkl	89.1	91.4	91	96.6	99.6
df	70.3	73.9	74.3	22.4	97.3
mel	90.1	92.8	92.8	94.1	98.6
nv	92.4	95.3	94.7	98.2	95.9
vasc	75.9	78.6	79.3	91.7	99.7
average ratio	**84.73**	**93.80**	**87.74**	**82.90**	**98.47**

Figure 10 shows the CM generated by the ANN with ResNet18 features to classify the ISIC2018 dataset. The ANN-ResNet18 achieved accuracy for each class: akiec of 90.8%, bcc of 91.3%, bkl of 91.4%, df of 73.9%, mel of 92.8%, nv of 95.3% and vasc of 78.6%.

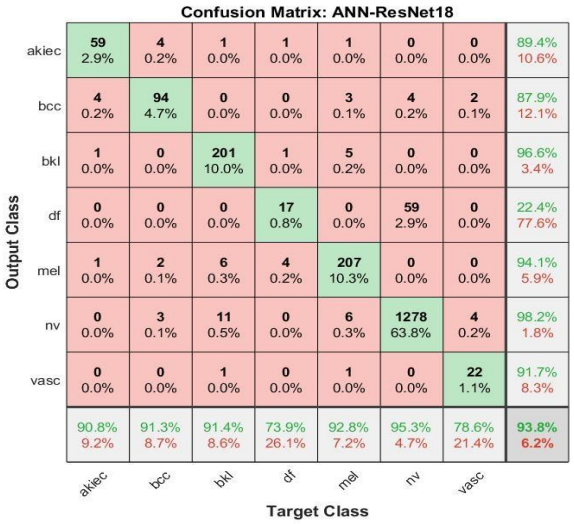

Fig.10. Display CM for results of ANN with ResNet18 features for classification on the ISIC2018 dataset.

F. Results of SVM with ResNet18 Features

The section discusses the performance of SVM with ResNet18 features for classification on the ISIC2018 dataset. The images were enhanced, ROI and deformities were isolated, and fed into ResNet18 model. The deep features of ResNet18 are fed to an SVM for classification.

Table 5 describes the performance of SVM with ResNet18 features for classifying the ISIC2018 dataset. SVM achieved an AUC of 80.63%, accuracy of 86.2%, sensitivity of 77.04%, precision of 67.59%, and specificity of 97.46%

TABLE 5. RESULTS OF SVM WITH RESNET18 FEATURES FOR CLASSIFICATION ON THE ISIC2018 DATASET

Type of Class	AUC %	Accuracy %	Sensitivity %	Precision %	Specificity %
akiec	75.6	78.5	78.3	70.8	99.2
bcc	86.2	89.3	88.7	80	98.6
bkl	91.3	95.5	95.4	50.5	88.2
df	90.8	95.7	96.1	88	99.5
mel	52.6	0	0	0	100
nv	88.3	99.1	99.2	98.6	97.2
vasc	79.6	82.1	81.6	85.2	99.5
average ratio	**80.63**	**86.20**	**77.04**	**67.59**	**97.46**

Figure 11 shows the CM generated by the SVM with ResNet18 features to classify the ISIC2018 dataset. The SVM-ResNet18 achieved accuracy for each class: akiec of

78.5%, bcc of 89.3%, bkl of 95.5%, df of 95.7%, nv of 99.1% and vasc of 82.1%.

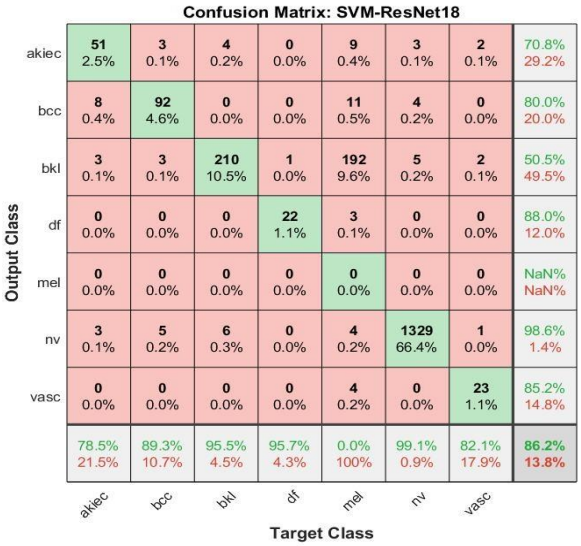

Fig.11. Display CM for results of SVM with ResNet18 features for classification on the ISIC2018 dataset.

V. DISCUSSION AND COMPARISON OF PERFORMANCE

Early diagnosis of SL is important for timely treatment and saving lives from the danger of melanoma. AI technologies including ML and DL have emerged as powerful tools for early diagnosis of SL. ML and DL technologies provide high capabilities and efficiencies to discover patterns, distortions, and hidden signs that doctors do not notice. ML and DL are also capable of processing large amounts of images quickly and effectively, allowing effective examination of clinical environments. In this study, HF were extracted by GLCM, LBP, and FCH. GLCM determines the spatial relationships between pairs of pixels while LBP captures the texture patterns of binary surfaces. FCH works to extract color features by distributing colors in the fuzzy system on the histogram bin. By integrating features from several methods allows a system to benefit from complementary information. The hybrid systems ANN-ResNet18 and SVM-ResNet18 combine ResNet18's feature-rich deep feature extraction and classification by ANN and SVM. ANN is characterized by capturing complex nonlinear relationships while SVM is effective in determining decision boundaries between various classes of the ISIC 2018 dataset. ANN-ResNet18 achieved promising results, reaching an AUC of 84.73%, sensitivity of 87.74%, accuracy of 93.8%, precision of 82.9%, and specificity of 98.47%.

Previous studies have applied various DL, ML and VR image processing models such as upsampling, dropout, transfer learning and data augmentation to classify SL, with accuracy ranging from 73.2% to 90.4%. The proposed systems use HF extracted from GLCM, LBP, and FCH methods, combined with ResNet18 features, and classified using ANN and SVM. The two ANN-ResNet18 hybrid systems achieved superior results with an AUC of 84.73%, sensitivity of 87.74%, accuracy of 93.8%, precision of 82.9%, and specificity of 98.47%.

TABLE 6. COMPARISON OF THE RESULTS OF THE PROPOSED SYSTEM WITH PREVIOUS STUDIES

Study	Techniques	Results
Soudani et al.	VGG-16, ResNet-50, downsampling, dropout	VGG-16: 76.3%, ResNet-50: 73.2%
Mabrouk et al.	Image preprocessing, density regression, SVM, KNN, ANN	ANN: >90%
Gong et al.	Transfer learning, normalization, ensemble CNN	Accuracy: 90.4%, Sensitivity: 45%, Specificity: 93.7%
Birkenfeld et al.	Otsu method, ABCD rule, logistic regression	Sensitivity: 83.2%
Fekry et al.	Image enhancement, segmentation, CNN, RF	AUC: 87.98%, Sensitivity: 80.4%
Naeem et al.	Anisotropic diffusion, SMOTE, VGG19	Accuracy: 77.97%, Sensitivity: 69.49%
Kaur et al.	CNN, lesion segmentation	ISIC2016 Jaccard: 90.4%, ISIC2018 Jaccard: 89.1%
Proposed system	ANN-ResNet18	an AUC of 84.73%, sensitivity of 87.74%, accuracy of 93.8%, precision of 82.9%, and specificity of 98.47%.

The proposed system achieves high performance compared to previous studies, as shown in Table 6. It outperforms models such as ResNet-50 and VGG-16 from Sudani and others, as it achieved an accuracy of 93.8%. It also achieved a high sensitivity of 87.74%, indicating its efficiency in identifying true positive TP cases. Moreover, the specificity of 98.47% indicates its ability to identify true negative TN cases. Overall, the proposed system effectively combines features from different techniques to achieve robust performance across multiple evaluation metrics.

VI. CONCLUSION

Nowadays, there should be widespread interest in detecting the most serious skin diseases. Systems based on hybrid features have been developed to diagnose images in the early stages. The images were enhanced to remove artifacts and the ACA algorithm was applied to extract areas of lesions and deformities and isolate them from healthy areas. The areas of lesions and deformities were fed into two strategies: The first strategy relies on extracting features from the GLCM, LBP and FCH algorithms and merging them. The fused features were fed to the ANN and SVM classifiers for classification with high accuracy. The second strategy relies on the ResNet18 model to extract deep features and classify them very efficiently using ANN and SVM classifiers. The ANN-

ResNet18 strategy achieved an AUC of 84.73%, sensitivity of 87.74%, accuracy of 93.8%, precision of 82.9%, and specificity of 98.47%.

ACKNOWLEDGMENT:

The authors are thankful to the presidency of Al-Razi University and the Scientific Research Center for facilitating the completion of this study.

REFERENCES

[1] R. Jin, L. Luo, and J. Zheng, "The Trinity of Skin: Skin Homeostasis as a Neuro–Endocrine–Immune Organ," *Life 2022, Vol. 12, Page 725*, vol. 12, no. 5, p. 725, May 2022, doi: 10.3390/LIFE12050725.

[2] C. Zhang, G. R. Merana, T. Harris-Tryon, and T. C. Scharschmidt, "Skin immunity: dissecting the complex biology of our body's outer barrier," *Mucosal Immunol*, vol. 15, no. 4, pp. 551–561, Apr. 2022, doi: 10.1038/S41385-022-00505-Y.

[3] M. Vestita, P. Tedeschi, and D. Bonamonte, "Anatomy and Physiology of the Skin," *Textbook of Plastic and Reconstructive Surgery: Basic Principles and New Perspectives*, pp. 3–13, Jan. 2022, doi: 10.1007/978-3-030-82335-1_1.

[4] M. Emanuelli *et al.*, "The Double-Edged Sword of Oxidative Stress in Skin Damage and Melanoma: From Physiopathology to Therapeutical Approaches," *Antioxidants 2022, Vol. 11, Page 612*, vol. 11, no. 4, p. 612, Mar. 2022, doi: 10.3390/ANTIOX11040612.

[5] N. H. Khan *et al.*, "Skin cancer biology and barriers to treatment: Recent applications of polymeric micro/nanostructures," *J Adv Res*, vol. 36, pp. 223–247, Feb. 2022, doi: 10.1016/J.JARE.2021.06.014.

[6] P. Chauhan, R. Jindal, and E. Errichetti, "Dermoscopy of skin parasitoses, bites and stings: a systematic review of the literature," *Journal of the European Academy of Dermatology and Venereology*, vol. 36, no. 10, pp. 1722–1734, Oct. 2022, doi: 10.1111/JDV.18352.

[7] G. Arora, A. K. Dubey, Z. A. Jaffery, and A. Rocha, "Bag of feature and support vector machine based early diagnosis of skin cancer," *Neural Comput Appl*, vol. 34, no. 11, pp. 8385–8392, Jun. 2022, doi: 10.1007/S00521-020-05212-Y/METRICS.

[8] K. A. Muhaba, K. Dese, T. M. Aga, F. T. Zewdu, and G. L. Simegn, "Automatic skin disease diagnosis using deep learning from clinical image and patient information," *Skin Health and Disease*, vol. 2, no. 1, p. e81, Mar. 2022, doi: 10.1002/SKI2.81.

[9] K. Szturo, J. Haueisen, and L. Piatek, "MSLO - Melanocytic skin lesion ontology," *Digit Med*, vol. 8, p. 29, Jan. 2022, doi: 10.4103/DIGM.DIGM_18_22.

[10] S. Chakraborty and K. Mali, "An Overview of Biomedical Image Analysis From the Deep Learning Perspective," *https://services.igi-global.com/resolvedoi/resolve.aspx?doi=10.4018/978-1-6684-7544-7.ch003*, pp. 43–59, Jan. 1AD, doi: 10.4018/978-1-6684-7544-7.CH003.

[11] R. F. Mansour, N. M. Alfar, S. Abdel-Khalek, M. Abdelhaq, R. A. Saeed, and R. Alsaqour, "Optimal deep learning based fusion model for biomedical image classification," *Expert Syst*, vol. 39, no. 3, p. e12764, Mar. 2022, doi: 10.1111/EXSY.12764.

[12] A. Soudani and W. Barhoumi, "An image-based segmentation recommender using crowdsourcing and transfer learning for skin lesion extraction," *Expert Syst Appl*, vol. 118, pp. 400–410, Mar. 2019, doi: 10.1016/J.ESWA.2018.10.029.

[13] L. Liu, L. Mou, X. X. Zhu, and M. Mandal, "Automatic skin lesion classification based on mid-level feature learning," *Computerized Medical Imaging and Graphics*, vol. 84, p. 101765, Sep. 2020, doi: 10.1016/J.COMPMEDIMAG.2020.101765.

[14] F. Pollastri, F. Bolelli, R. Paredes, and C. Grana, "Augmenting data with GANs to segment melanoma skin lesions," *Multimed Tools Appl*, vol. 79, no. 21–22, pp. 15575–15592, Jun. 2020, doi: 10.1007/S11042-019-7717-Y/FIGURES/13.

[15] M. S. Mabrouk, A. Y. Sayed, H. M. Afifi, M. A. Sheha, and A. Sharwy, "Fully Automated Approach for Early Detection of Pigmented Skin Lesion Diagnosis Using ABCD," *Journal of Healthcare Informatics Research 2020 4:2*, vol. 4, no. 2, pp. 151–173, Mar. 2020, doi: 10.1007/S41666-020-00067-3.

[16] A. Gong, X. Yao, and W. Lin, "Dermoscopy Image Classification Based on StyleGANs and Decision Fusion," *IEEE Access*, vol. 8, pp. 70640–70650, 2020, doi: 10.1109/ACCESS.2020.2986916.

[17] J. S. Birkenfeld, J. M. Tucker-Schwartz, L. R. Soenksen, J. A. Avilés-Izquierdo, and B. Marti-Fuster, "Computer-aided classification of suspicious pigmented lesions using wide-field images," *Comput Methods Programs Biomed*, vol. 195, p. 105631, Oct. 2020, doi: 10.1016/J.CMPB.2020.105631.

[18] F. Olayah, E. M. Senan, I. A. Ahmed, and B. Awaji, "AI Techniques of Dermoscopy Image Analysis for the Early Detection of Skin Lesions Based on Combined CNN Features," *Diagnostics 2023, Vol. 13, Page 1314*, vol. 13, no. 7, p. 1314, Apr. 2023, doi: 10.3390/DIAGNOSTICS13071314.

[19] A. Naeem and T. Anees, "DVFNet: A deep feature fusion-based model for the multiclassification of skin cancer utilizing dermoscopy images," *PLoS One*, vol. 19, no. 3, p. e0297667, Mar. 2024, doi: 10.1371/JOURNAL.PONE.0297667.

[20] A. Naeem, T. Anees, M. Fiza, R. A. Naqvi, and S. W. Lee, "SCDNet: A Deep Learning-Based Framework for the Multiclassification of Skin Cancer Using Dermoscopy Images," *Sensors 2022, Vol. 22, Page 5652*, vol. 22, no. 15, p. 5652, Jul. 2022, doi: 10.3390/S22155652.

[21] R. Kaur, H. GholamHosseini, R. Sinha, and M. Lindén, "Automatic lesion segmentation using atrous convolutional deep neural networks in dermoscopic skin cancer images," *BMC Med Imaging*, vol. 22, no. 1, pp. 1–13, Dec. 2022, doi: 10.1186/S12880-022-00829-Y/FIGURES/8.

[22] P. Tschandl *et al.*, "Human–computer collaboration for skin cancer recognition," *Nat Med*, vol. 26, no. 8, pp. 1229–1234, Aug. 2020, doi: 10.1038/S41591-020-0942-0.

[23] I. A. Ahmed *et al.*, "Multi-Techniques for Analyzing X-ray Images for Early Detection and Differentiation of Pneumonia and Tuberculosis Based on Hybrid Features," *Diagnostics 2023, Vol. 13, Page 814*, vol. 13, no. 4, p. 814, Feb. 2023, doi: 10.3390/DIAGNOSTICS13040814.

[24] E. Goceri, "Evaluation of denoising techniques to remove speckle and Gaussian noise from dermoscopy images," *Comput Biol Med*, vol. 152, p. 106474, Jan. 2023, doi: 10.1016/J.COMPBIOMED.2022.106474.

[25] A. Khalid, E. M. Senan, K. Al-Wagih, M. M. Ali Al-Azzam, and Z. M. Alkhraisha, "Hybrid Techniques of X-ray Analysis to Predict Knee Osteoarthritis Grades Based on Fusion Features of CNN and Handcrafted," *Diagnostics 2023, Vol. 13, Page 1609*, vol. 13, no. 9, p. 1609, May 2023, doi: 10.3390/DIAGNOSTICS13091609.

[26] Y. S. Malik, M. Tamoor, A. Naseer, A. Wali, and A. Khan, "Applying an adaptive Otsu-based initialization algorithm to optimize active contour models for skin lesion segmentation," *J Xray Sci Technol*, vol. 30, no. 6, pp. 1169–1184, Jan. 2022, doi: 10.3233/XST-221245.

[27] E. M. Senan, M. E. Jadhav, and A. Kadam, "Classification of PH2 Images for Early Detection of Skin Diseases," *2021 6th International Conference for Convergence in Technology, I2CT 2021*, Apr. 2021, doi: 10.1109/I2CT51068.2021.9417893.

[28] S. M. Fati, E. M. Senan, and Y. Javed, "Early Diagnosis of Oral Squamous Cell Carcinoma Based on Histopathological Images Using Deep and Hybrid Learning Approaches," *Diagnostics*, vol. 12, no. 8, p. 1899, Aug. 2022, doi: 10.3390/DIAGNOSTICS12081899.

[29] E. M. Senan and M. E. Jadhav, "Techniques for the Detection of Skin Lesions in PH2 Dermoscopy Images Using Local Binary Pattern (LBP)," *Communications in Computer and Information Science*, vol. 1381 CCIS, pp. 14–25, 2021, doi: 10.1007/978-981-16-0493-5_2.

[30] M. Al-Jabbar, M. Alshahrani, E. M. Senan, and I. A. Ahmed, "Histopathological Analysis for Detecting Lung and Colon Cancer Malignancies Using Hybrid Systems with Fused Features," *Bioengineering 2023, Vol. 10, Page 383*, vol. 10, no. 3, p. 383, Mar. 2023, doi: 10.3390/BIOENGINEERING10030383.

[31] H. K. Gajera, D. R. Nayak, and M. A. Zaveri, "A comprehensive analysis of dermoscopy images for melanoma detection via deep CNN features," *Biomed Signal Process Control*, vol. 79, p. 104186, Jan. 2023, doi: 10.1016/J.BSPC.2022.104186.

[32] I. A. Ahmed, E. M. Senan, and H. S. A. Shatnawi, "Analysis of Histopathological Images for Early Diagnosis of Oral Squamous Cell Carcinoma by Hybrid Systems Based on CNN Fusion Features," *International Journal of Intelligent Systems*, vol. 2023, 2023, doi: 10.1155/2023/2662719.

[33] A. Bibi *et al.*, "Skin Lesion Segmentation and Classification Using Conventional and Deep Learning Based Framework", doi: 10.32604/cmc.2022.018917.

[34] A. Shah *et al.*, "A comprehensive study on skin cancer detection using artificial neural network (ANN) and convolutional neural network (CNN)," *Clinical eHealth*, vol. 6, pp. 76–84, Dec. 2023, doi: 10.1016/J.CEH.2023.08.002.

[35] E. A. Alshari and B. W. Gawali, "Analysis of Machine Learning Techniques for Sentinel-2A Satellite Images," *Journal of Electrical and Computer Engineering*, vol. 2022, 2022, doi: 10.1155/2022/9092299.

[36] D. Keerthana, V. Venugopal, M. K. Nath, and M. Mishra, "Hybrid convolutional neural networks with SVM classifier for classification of skin cancer," *Biomedical Engineering Advances*, vol. 5, p. 100069, Jun. 2023, doi: 10.1016/J.BEA.2022.100069.

[37] A. Shamsan, E. M. Senan, and H. S. A. Shatnawi, "Automatic Classification of Colour Fundus Images for Prediction Eye Disease Types Based on Hybrid Features," *Diagnostics 2023, Vol. 13, Page 1706*, vol. 13, no. 10, p. 1706, May 2023, doi: 10.3390/DIAGNOSTICS13101706.

التشخيص المبكر لآفات الجلد متعددة الفئات باستخدام نماذج هجينة على أساس الميزات المندمجة

إبراهيم محمد سنان
قسم نظم المعلومات ، كلية علوم الحاسب وتكنولوجيا المعلومات ، جامعة الرازي ، صنعاء ، اليمن
senan1710@gmail.com

خليل الوجيه
قسم الذكاء الاصطناعي ، كلية علوم الحاسب وتكنولوجيا المعلومات ، جامعة الرازي ، صنعاء ، اليمن
khalilwagih@gmail.com

إيمان أحمد الشهاري
قسم نظم المعلومات ، كلية علوم الحاسب وتكنولوجيا المعلومات ، جامعة الرازي ، صنعاء ، اليمن
em.alshari3@gmail.com

ملخص البحث

الأنواع الخطيرة من آفات الجلد . يزداد معدل حدوث سرطان الجلد من النوع الميلاني سنوياً ، مما يشكل خطراً صحياً يهدد الحياة. تعتبر التصوير المجهري الجلدي (الديرموسكوبي) إحدى أفضل التقنيات التي تكشف عن البنى الداخلية غير المرئية وتساعد في الكشف عن أنواع آفات الجلد . تتشابه آفات الجلد في مراحلها المبكرة ، مما يشكل تحدياً في التمييز بينها بالتشخيص اليدوي. لذلك ، تعالج تقنيات الذكاء الاصطناعي هذه الثغرات من خلال التشخيص ISIC اليدوي. في هذه الدراسة ، تم تطوير استراتيتجيتين لتحليل الصور الديرموسكوبية للتشخيص المبكر لآفات الجلد . تم تحسين الصور من أجل تحدي وعزلها عن المناطق الصحية. تم تغذية منطقة الاهتمام (ROI) لاستخراج مناطق الاهتمام (ACA) ، وطُبق خوارزمية المخطط النشط2018 بشكل منفصل إلى الاستراتيجيتين. تلقت الاستراتيجية الأولى منطقة الاهتمام وتم تغذيتها بخوارزميات مصفوفة التشابه ذات المستوى الرمادي لاستخراج الميزات. تم دمجها في متجهات الميزات. تم تغذية الميزات (FCH) ومؤشر اللون الضبابي (LBP) والنمط الثنائي المحلي (GLCM) لتصنيفها بدقة عالية. تلقت الاستراتيجية الثانية منطقة (SVM) والآلة الناقلة للدعم (ANN) المندمجة إلى محلل الشبكة العصبية الاصطناعية ANN- حقق .SVM و ANN لاستخراج الميزات العميقة وتصنيفها بكفاءة كبيرة باستخدام ResNet18 الاهتمام وتم تغذيتها إلى نموذج بنسبة 84.73٪ ، وحساسية 87.74٪ ، ودقة 93.8٪ ، وتوقع 82.9٪ ، وتحديد نوعية AUC نتائج واعدة ، حيث وصل إلى ResNet18 ٪98.47.

الكلمات الرئيسية: SVM; ANN; CNN; **دمج الميزات**; **آفة الجلد**; HF